

Oil Phase Velocity Measurement of Oil-Water Two-Phase Flow with Low Velocity and High Water Cut Using the Improved ORB and RANSAC Algorithm

Lianfu Han^{1,2}, Haixia Wang^{1,3}, Yao Cong¹, Xingbin Liu², Jian Han¹, Changfeng Fu^{1,*}

¹*College of Electronics Science, Northeast Petroleum University, Fazhan road No.199, 163316, Daqing, China Institute,*

^{*}*changfengfu@nepu.edu.cn*

²*Working Stations for Post Doctor, Daqing Oilfield Limited Corporation, XiBin Road, No.110, 163310, Daqing, China*

³*College of Electrical and Information Engineering, Tianjin University, Weijin Road, No.92, 300072, Tianjin, China*

Velocity is an important parameter for fluid flow characteristics in profile logging. Particle tracking velocimetry (PTV) technology is often used to study the flow characteristics of oil wells with low flow velocity and high water cut, and the key to PTV technology is particle matching. The existing particle matching algorithms of PTV technology do not meet the matching demands of oil drops in the oil phase velocity measurement of oil-water two-phase flow with low velocity and high water cut. To raise the particle matching precision, we improved the particle matching algorithm from the oriented FAST and the rotated BRIEF (ORB) feature description and the random sample consensus (RANSAC) algorithm. The simulation and experiment were carried out. Simulation results show that the improved algorithm not only increases the number of matching points but also reduces the computation. The experiment shows that the improved algorithm in this paper not only reduces the computation of the feature description process, reaching half of the computation amount of the original algorithm, but also increases the number of matching results, thus improving the measurement accuracy of oil phase velocity. Compared with the SIFT algorithm and the ORB algorithm, the improved algorithm has the largest number of matching point pairs. And the variation coefficient of this algorithm is 0.039, which indicates that the algorithm is stable. The mean error of oil phase velocity measurement of the improved algorithm is 1.20 %, and the maximum error is 6.16 %, which is much lower than the maximum error of PTV, which is 25.89 %. The improved algorithm overcomes the high computation cost of the SIFT algorithm and achieves the precision of the SIFT algorithm. Therefore, this study contributes to the improvement of the measurement accuracy of oil phase velocity and provides reliable production logging data for oilfield.

Keywords: ORB, RANSAC, oil-water two-phase flow, PTV.

1. INTRODUCTION

Flow velocity [1] is an important monitoring parameter for oilfield development and it can evaluate the production of each oil reservoir [2]-[3]. Due to low velocity and high water cut, flow characteristics of oil-water two-phase flow [4]-[7] are very different from those of other conditions. The interpretation of log data [8]-[10] such as velocity depends on flow characteristics, so it is necessary to study the flow characteristics of oil-water two-phase flow at low flow velocity and high water cut state. PTV technology [11]-[12] is a common multiphase flow velocity measurement technology, which attracts the attention of many scholars. Fu et al. analyzed measurement performances of 3D-PTV and typical 2D-particle image velocimetry (PIV) algorithm on laminar macroscopic flow with three known displacements, and applied two algorithms to the indoor low turbulence experiment generated by low-speed exhaust

pipes for comparison [13]. The results show that the 3D-PTV algorithm has better velocity measurement ability than the 2D-PIV algorithm when the tracking particle density is greater than 2 and the particle density increases gradually. Therefore, it can be known that the number of tracking particles is one of the important factors that determine the measurement accuracy of PTV technology.

The key to PTV technology [14] is to track the trajectory of characteristic particles and calculate their velocities, that is, to match the same particles at different times and calculate their velocities. The accuracy of particle matching directly affects measurement accuracy of flow characteristics [15], such as velocity. There are many ways to match particles, for example, Qin et al. proposed a transient feature extraction method based on improved orthogonal matching pursuit and the K-singular value decomposition (K-SVD) algorithm to detect early faults of

rotating parts in electromechanical systems [16]. Manickam et al. proposed the SIFT algorithm to enhance potential fingerprint matching to extend the fingerprint matching technology [17]. Ma et al. proposed an improved ORB algorithm based on the speeded up robust features (SURF) algorithm [18]. The experiment results show that the improved algorithm has strong robustness under complex conditions such as image blurring and noise interference. In the velocity measurement of oil-water two-phase flow, Kong et al. proposed a PTV algorithm based on the scale-invariant feature transform (SIFT) feature point matching, which was applied to velocity measurement of oil-water two-phase flow with low particle concentration [19]. The measurement results are of high precision and the method is applicable to oil droplet overlap and oil droplet size distribution. Yu et al. proposed an improved binary feature point extraction algorithm based on ORB [20], which was faster and more accurate than the SIFT and the SURF algorithms. SIFT algorithm has high accuracy, but the calculation process is complicated and takes a long time. The oil phase of oil-water two-phase flow at low flow velocity is distributed above the horizontal pipe, and oil phase slippage occurs under the influence of gravity and density [21]. Even under the same operating condition, this phenomenon cannot make the average velocity of oil-water two-phase flow replace the average velocity of oil-phase flow. So far, few studies have been done on oil phase velocity measurement alone. In addition, many scholars have studied and improved the ORB algorithm to improve its algorithm matching accuracy. For example, Pang et al. proposed an improved ORB feature point matching algorithm based on particle swarm optimization algorithm to improve the image matching accuracy [22]. Shu et al. firstly used the angle cosine method to conduct preliminary screening of matching point pairs, and then used the RANSAC algorithm based on homography matrix to eliminate false matching point pairs to improve the matching accuracy [23]. The improved algorithm is robust and not affected by image blurring and brightness unevenness. Many studies have been conducted in the direction of improving algorithm accuracy. PTV algorithm is to calculate the average velocity vector of particles based on the final result of the matching. It should not only consider the accuracy of the matching algorithm, but also consider the number of matching results. The greater the number of matching results, the closer the PTV algorithm's calculation results will be to the average particle velocity, and therefore, the higher the accuracy of the final velocity measurement will be.

Based on previous studies, the ORB algorithm was applied to calculate the oil phase velocity of oil-water two-phase flow with low flow velocity and high water cut, and the matching result was shown in Fig.1. The blue lines in the figure are the matching results of oil phase characteristics of the first and second images. The green points to the left of the blue lines are oil phase feature points in the first frame, and the red points on the right are oil phase feature points in the second frame. The ORB algorithm is an improvement on the Features from Accelerated Segment Test (FAST)

algorithm [24] and the Binary Robust Independent Elementary Features (BRIEF) algorithm [25]. Compared with the SIFT and the SURF algorithms, the calculation methods of the FAST algorithm and the BRIEF algorithm are relatively simple and the calculation amount is also less. The calculation amount is inversely proportional to the calculation speed. In addition, the Hamming distance is used for matching in the ORB algorithm, and the number of error matches is large. So, the ORB algorithm computes fast enough, but with very low accuracy.

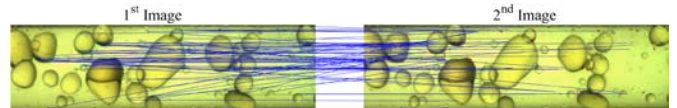


Fig.1. Oil-water two-phase flow oil matching results using the ORB algorithm.

Considering the efficiency and accuracy of the ORB and the RANSAC algorithms, a PTV algorithm based on the improved ORB and RANSAC algorithms was proposed in this paper to improve the measurement velocity accuracy of oil phase in oil-water two-phase flow with low velocity and high water cut. The research method is simple and the calculation is efficient and accurate, which is convenient to analyze the flow characteristics of oilfield fluid and interpret the logging data. However, it is suitable for the study of oil-phase velocity of oil-water two-phase flow with high water cut and low flow velocity. In this condition, the oil-phase in the fluid exists in a bubble and the oil-phase characteristic is extracted using the ORB algorithm to facilitate the calculation of oil-phase velocity.

First, the improvement of feature point description for ORB feature extraction and the RANSAC algorithm is described. Then, the improved algorithm is verified by simulation and experiment. Last, the improved algorithm is applied to measure the oil-phase velocity of oil-water two-phase flow with low flow velocity and high water cut, and the measurement results are analyzed.

2. ORB FEATURE EXTRACTION OF OIL PHASE

ORB feature extraction [26] is an improved algorithm based on the FAST algorithm and the BRIEF algorithm, including feature point detection and feature point description. In this paper, the feature point description of oil phase is improved.

To make feature point description distinguishable and improve the accuracy of subsequent matching, ORB feature point description [27]-[28] improves the BRIEF algorithm by adding rotation factor in the direction of feature points. The selection of randomly selected point pairs corresponding to a feature point descriptor in the ORB algorithm is shown in Fig.2.a). The point pairs are randomly selected in the region 31-by-31 center on feature points. The points are sorted out and defined as 2-by-2n dimensional matrix, which is named as point set matrix. And the matrix is fixed and consistent with all feature points in the image. Therefore, randomly selected point pairs should be rotated according to the direction of feature points, which extends the time used for feature point description.

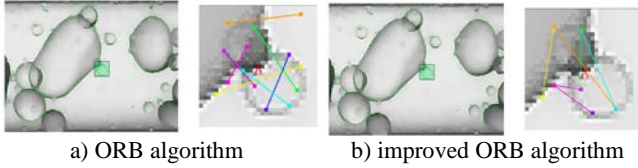


Fig.2. The selection of feature point descriptors.

This paper proposes a way to reduce the number of random points corresponding to descriptors to reduce the computing time of feature point description. Namely, a way to reduce the number of column vectors of matrix S . The algorithm steps of this paper are as follows:

Step 1: determine point set matrix S' . The second random point required by the l^{th} binary code is taken as the first random point required by the $(l+1)^{\text{th}}$ binary code, as shown in Fig.2.b). If the length of binary code string is n , then the number of column vectors of matrix S' is $n+1$. The matrix is expressed as (1):

$$S' = \begin{bmatrix} x_1 & x_2 & \cdots & x_{n+1} \\ y_1 & y_2 & \cdots & y_{n+1} \end{bmatrix} \quad (1)$$

As shown in Fig.2., column vectors number of matrix S' is reduced from $2n$ column vectors of matrix S to $n+1$. The computation of $S' \rightarrow S'_\theta$ is also reduced.

Step 2: determine the rotation matrix S'_θ . Rotate matrix S' according to rotation matrix R_θ corresponding to the direction of characteristic points θ , and equation (2) is obtained:

$$S'_\theta = R_\theta S' = \begin{bmatrix} \cos \theta & \sin \theta \\ -\sin \theta & \cos \theta \end{bmatrix} \begin{bmatrix} x_1 & x_2 & \cdots & x_{n+1} \\ y_1 & y_2 & \cdots & y_{n+1} \end{bmatrix} = [P_1 \ P_2 \ \cdots \ P_{n+1}] \quad (2)$$

According to (2), four multiplication operations and two addition operations are required to obtain each column in matrix S'_θ . Compared with the ORB algorithm, the improved ORB algorithm reduces the multiplication amount m_s and the addition quantity a_s . The decrease of the multiplication amount m_s and the addition quantity a_s are as follows:

$$\begin{cases} m_s = g \times 2n \times 4 - g \times (n+1) \times 4 = 4g(n-1) \\ a_s = g \times 2n \times 2 - g \times (n+1) \times 2 = 2g(n-1) \end{cases} \quad (3)$$

Where, g is the number of feature points in the image.

Step 3: determine the descriptors of feature points. Because the form of ORB descriptors is a binary code string, the descriptors at feature point $P_j(x_j, y_j)$ are shown in (4):

$$f_m = \sum_{1 \leq j \leq m} 2^{j-1} \tau_j \quad (4)$$

Where, m is the length of binary string descriptors, 256 is taken in this paper; τ_j is a binary code, as shown in (5).

$$\tau_j = \begin{cases} 1, & I'(P_j) < I'(P_{j+1}) \\ 0, & I'(P_j) \geq I'(P_{j+1}) \end{cases}, j = 1, 3, 5, \dots, 2n-1 \quad (5)$$

Where, $I'(P_j)$ is the smoothed pixel value at point $P_j(x_j, y_j)$.

ORB descriptors are independent of location and pixel value of selected random points, and they are related to the pixel values difference of two points. Stability of descriptors is determined by the greedy algorithm. Therefore, the decrease of random points number does not affect the stability of binary code string descriptors. The improved ORB algorithm is named as oriented FAST and Continuous rotated BRIEF algorithm, shortened as OCRB algorithm.

3. OIL PHASE FEATURE MATCHING IMPROVEMENT

Only Hamming distance is used to match the extracted feature points after ORB feature extraction. In other words, the point pairs with the smallest Hamming distance are selected as the matching point pairs. The matching point pairs of all oil phases are shown in Fig.3. The blue lines in the figure are the matching results of oil phase characteristics of the first and second images. The green points to the left of the blue lines are the oil phase feature points in the first frame, and the red points on the right are the oil phase feature points in the second frame.

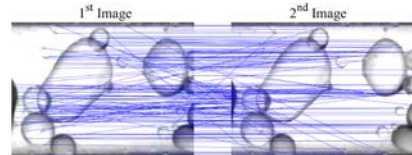


Fig.3. Feature point matching results of oil phase.

Oil phase feature point matching results are divided into the following three matching types: 1) Correct matching point pairs. As shown in Fig.4.a), the similarity of feature points of the two images is the highest, and there is no feature point more similar than the other. 2) Wrong matching point pairs caused by high peripheral similarity. As shown in Fig.4.b), even if the similarity around some feature points in the two frames is the highest, wrong matching also occurs. 3) Wrong matching point pairs caused by repeated matching. As shown in Fig.4.c), it is obvious that some feature points in the first image have no corresponding and correctly matched feature points in the second image. So the feature points with the highest similarity are directly selected as matching point pairs according to the Hamming distance criterion. Repeated matching of one feature point will be formed, in which there's bound to be a false match.

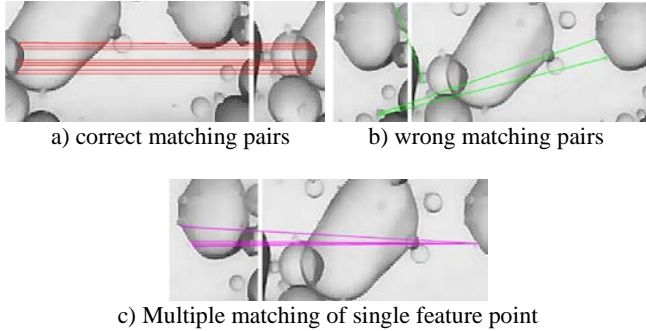


Fig.4. Oil phase feature point matching results classification.

For these three matching types, it is urgent to eliminate wrong matching point pairs to improve matching accuracy. The RANSAC algorithm [29]-[31] is often used to eliminate wrong matching points, and has noise resistance and robustness. Correct matching point pairs are still obtained after several iterations for data containing a large number of wrong matches.

Before the calculation of the RANSAC algorithm, the data with low similarity but correct matching were removed in the process of determining the observed data and model calculation data of the RANSAC algorithm, so the recall rate of the RANSAC algorithm was far less than 1. So the RANSAC algorithm does not perform well. Due to the instability of flow velocity of oil-water two-phase flow, the local velocity cannot represent the overall velocity. The more point pairs that match, the more accurate the average oil phase velocity in oil-water two-phase flow is. Therefore, the RANSAC algorithm is improved.

A. Improved RANSAC algorithm

To obtain more correct data of matching point pairs, observation data and model calculation data of the RANSAC algorithm are extracted separately, as shown in Fig.5.

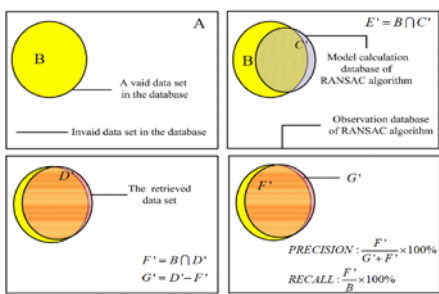


Fig.5. Analysis of improved RANSAC algorithm.

In Fig.5., B is all valid data in the data, that is, the correct matching point pairs in all matched data. A is all invalid data in the data, that is, the wrong matching point pairs in all matched data. O is all data, that is, all matching data, including correct matching point pairs and wrong matching point pairs, and the expression of O is $O=A\cup B$. Meanwhile, O serves as an improved RANSAC algorithm for observation data. As the model calculation data of the

improved RANSAC algorithm, C' satisfies two conditions: 1) it belongs to observation data; 2) the probability of the data being correctly matched is high enough. After repeated calculation and model fitting in C' data, the best model is selected, and has the largest number of corresponding inlier points in the model calculation data. The model is applied to the observation data to obtain the corresponding inlier points D' in the observation data, that is, the final matching point pairs. Where, F' and G' are, respectively, the correct matching point pairs and the wrong matching point pairs in the final matching point pairs D' . This algorithm is named as partial random sample consensus algorithm, and it is called PRANSAC algorithm for short. The precision and recall rate of the PRANSAC algorithm are, respectively:

$$\begin{cases} p' = \frac{F'}{G' + F'} \times 100\% = \frac{F'}{D'} \times 100\% \\ R' = \frac{F'}{B} \times 100\% \end{cases} \quad (6)$$

Comparing the RANSAC algorithm with the PRANSAC algorithm, the accuracy p' of the PRANSAC algorithm and p of the RANSAC algorithm are determined and obtained by confidence coefficient. Therefore, the accuracy of the two algorithms is not affected by the algorithm before and after the improvement. The ratio of the two recall rates r :

$$r = \frac{R'}{R} = \frac{F'/B}{F/B} = \frac{F'}{F} \quad (7)$$

The model calculation data and observation data of the RANSAC algorithm are C' , the model calculation data of the PRANSAC algorithm is C' , and the observation data is O . Obviously, due to the different observation data of the two algorithms, the matching point pairs retrieved from the model are different. Obviously, the correct matching data F' and F finally retrieved are different in size due to different observation data. The observation data of the former is larger than that of the latter, and the ratio of the recall rate r is greater than 1, so the size of the correct matching data retrieved by the former is also greater than that of the latter.

The improved feature matching is the final matching data processed by the Hamming distance and the PRANSAC algorithm. The algorithm steps are as follows:

Step 1: Extract the model calculation data C' in the PRANSAC algorithm. First, Hamming distance is used to conduct inverse matching of feature points, and data with bidirectional matching is retained. Then, the threshold of the Hamming distance is set to extract the data below the threshold, which is the model calculation data C' of the PRANSAC algorithm.

Step 2: The observation data O and model calculation data C' are normalized to reduce noise interference, so that the average distance [32] from each feature point to its shape point is $\sqrt{2}$. The transformation matrix is as follows:

$$H_{ij} = \begin{bmatrix} s & 0 & -s \times c_x \\ 0 & s & -s \times c_y \\ 0 & 0 & 1 \end{bmatrix}, i, j = 1, 2 \quad (8)$$

Where, i is the i^{th} image, $j = 1$ refers to observation data, $j = 2$ refers to model calculation data, c_x and c_y are the mean values of the horizontal and vertical coordinates of all feature points, respectively. s [33] refers to normalized stretch ratio, which is shown in (9):

$$s = \frac{\sqrt{2}}{\sqrt{(x - c_x)^2 + (y - c_y)^2}} \quad (9)$$

Where, x and y refer to the horizontal and vertical coordinates of feature points, respectively.

Step 3: Randomly select the data in model calculation data C' , use the extracted data to estimate the model according to (10). The basic matrix F' is obtained.

$$p_2^T F' p_1 = [x_2 \ y_2 \ 1] \begin{bmatrix} f_1 & f_2 & f_3 \\ f_4 & f_5 & f_6 \\ f_7 & f_8 & f_9 \end{bmatrix} \begin{bmatrix} x_1 \\ y_1 \\ 1 \end{bmatrix} = 0 \quad (10)$$

Where, p_2 is feature point of the second image matched by feature point p_1 in the first image.

Step 4: F' is inversely normalized and transformed to obtain the basic matrix F that conforms to observation data:

$$F = (H_{12}^{-1})^T (H_{22})^T F' H_{21} H_{11}^{-1} \quad (11)$$

Step 5: The distance from model calculation data to its polar line is calculated. A threshold is set for the distance, which is lower than the threshold is judged as the inner point. Otherwise, it is judged as the outer point. The number of points in the record is m .

Step 6: Repeat steps 4 and 5 for k times. If the number of iterations k has not reached k_{\max} and the optimal model has been determined, the iteration is terminated. The inlier points corresponding to the optimal model are selected as the matching point pairs finally obtained. If the number of iterations k has reached k_{\max} and the optimal model has not been determined, the iteration is terminated. The optimal model selects the best model at present, and its corresponding inlier points are the matching point pairs finally obtained. Where, k_{\max} is set to 1000 in this paper.

OCRB feature extraction and feature matching based on the PRANSAC algorithm in this paper are combined and named as P-OCRB algorithm.

4. THE P-OCRB ALGORITHM VERIFICATION

To verify the superiority of the P-OCRB algorithm, it is evaluated from aspects of description time, matching number and registration performance by taking Fig.6. as an example. In addition, the length of feature description time is related to and proportional to the amount of calculation in the process. The greater the amount of computation involved in feature description, the longer the description time will take. Therefore, the description time in this paper is reacted with the computational amount in the process.

A. Calculation amount of feature descriptions

The feature points in Fig.6. are extracted and described, and results are shown in Fig.7. and Table 1. The colored circles in Fig.7. are feature points extracted by the OCRB algorithm in Fig.6.



Fig.6. Algorithm validation image.



Fig.7. Verification image after extracting feature points.

According to Table 1., the descriptors calculation account of the ORB algorithm is 1.99 times that of the OCRB algorithm, which is approximately 2 times. It shows that the OCRB algorithm has great improvement in computational efficiency. And the correlation between feature points is small, which has little influence on subsequent feature matching. Therefore, the OCRB algorithm proposed in this paper is effective and feasible.

Table 1. Feature extraction and description.

Algorithm	Number of feature points	The computation of single feature point descriptors	The computation of all feature point descriptors
ORB algorithm	866	512	443392
OCRB algorithm	866	257	222562

B. Number of feature matching point pairs and matching accuracy

Feature matching is carried out according to the above feature extraction and description. First, all the feature points are matched in the forward direction and the reverse direction, and the feature points with bidirectional matching are preserved. The preserved feature points are matched one by one. Then, matching point pairs with similarity greater than 90 % are extracted from them. In other words, the threshold of the Hamming distance is set to 26 and matching point pairs with the Hamming distance lower than 26 are extracted. To clearly observe the difference between the R-ORB algorithm and the P-OCRB algorithm, the observed data and model calculation data in the R-ORB algorithm are matching point pairs obtained by the bidirectional matching and similarity of more than 90 %. The observed data in the P-OCRB algorithm are the matching point pairs obtained by the bidirectional matching, and the calculated data of the model are the matching point pairs obtained by the bidirectional matching and the similarity of more than 90 %. The matching results are shown in Fig.8.

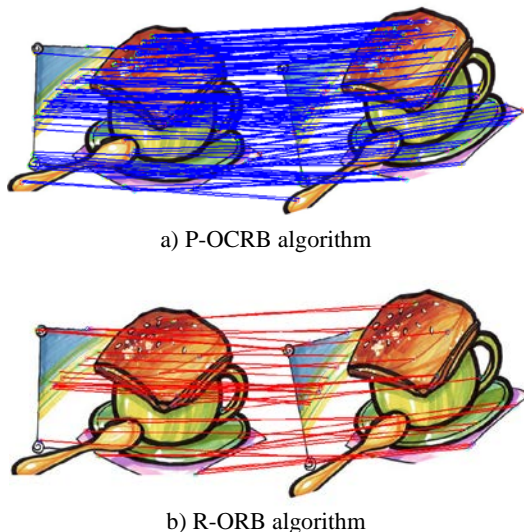


Fig.8. The matching results of validation image.

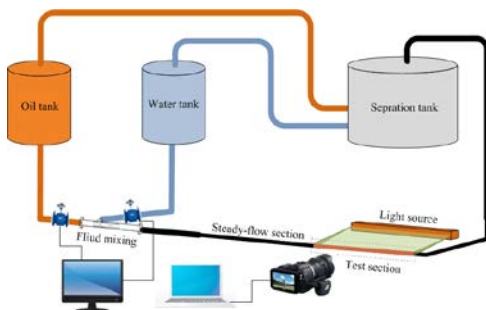
The number of matching point pairs obtained by the P-OCRB algorithm and the R-ORB algorithm is 308 pairs and 40 pairs, respectively. The number of matching point pairs of the former is significantly higher than that of the latter in Fig.8. Apparently, the P-OCRB algorithm has made a great breakthrough in the number of matching point pairs. Since the model calculation data of the two algorithms of PRANSAC and RANSAC are consistent, the optimal model selected is the same. The inlier points corresponding to the model are the matching point pairs finally obtained. Therefore, the accuracy of the selected optimal model determines the accuracy of the obtained matching point pairs. The matching effect of both algorithms is correct on the whole, and there is no wrong matching. Because the correct matching probability of the two algorithms is similar, the improvement of the algorithm has little effect on the accuracy. The P-OCRB algorithm can retain the high

accuracy of the original algorithm while extracting a large number of correct matching data.

To sum up, if matching data of the P-OCRB and the R-ORB algorithms achieve the same accuracy, the number of final matches obtained by the R-ORB algorithm is much less than that by the P-OCRB algorithm. If the same number of matches is extracted using two algorithms, the accuracy of the final matches obtained by the R-ORB algorithm is lower than that of the P-OCRB algorithm. Therefore, the P-OCRB algorithm has more reliability and superiority than the R-ORB algorithm.

5. EXPERIMENT

The experiment device for oil phase velocity measurement system is shown in Fig.9., which is composed of oil tank, water tank, oil-water separation tank, control system, and high-speed image acquisition module. The experiments are carried out in the simulated well of Daqing oilfield test service branch, and the image acquisition of the horizontal oil-water two-phase flow with high water cut and low velocity is conducted on the ground. According to the measurement requirements, the control system stirs and mixes the oil in the oil tank and the water in the water tank in a certain proportion. The mixed oil-water two-phase flow goes through the steady flow part and the test part, and then the oil-water two-phase flow is transported to the separation tank for oil-water separation, and finally to the oil tank and the water tank, respectively. In the test part, the images of oil-water two-phase flow are acquired by a high-speed camera.



a) chematic diagram of oil phase measurement using PTV.



b) physical diagram of oil phase measurement using PTV.

Fig.9. Experiment device for oil phase velocity measurement.

In the experiment, the fluid temperature is controlled at 77°F. Oil phase is white oil with a density of 0.8 g/cm³, and the water phase is tap water with a density of 0.99 g/cm³. The Reynolds number range of the oil phase is 914-4620. The pipe length of the steady flow part is 2 m, the pipe length of the test part is 0.1 m, and the pipe diameter is 0.02 m. The acquisition system adopts HVISION Macrovis

EoSens with a frame speed of 0.001 s. The image resolution obtained is 1280 pixels \times 1066 pixels. To test the reliability of the P-OCRB algorithm for measuring oil phase velocity of oil-water two-phase flow, the control platform was used to control velocity and water cut of oil-water two-phase flow. The total velocity range is 0.092 m/s~1.105 m/s, and the water cut is 70 %~90 %.

6. RESULTS AND DISCUSSION

As shown in Fig.10., oil phase images of oil-water two-phase flow based on PTV are randomly selected for processing according to the differences in flow velocity and water cut. They are, respectively, the flow with velocity of 0.368 m/s and water cut of 80 %, the fluid with velocity of 0.368 m/s and water cut of 90 %, the fluid with velocity of 0.553 m/s and water cut of 90 %, and the fluid with velocity of 0.737 m/s and water cut of 90 %. To verify the effectiveness and feasibility of the improved algorithm in oil-water two-phase flow, the P-OCRB, the R-ORB, and the R-SIFT (To facilitate subsequent comparison, Euclidean distance is used for matching after feature extraction by the SIFT algorithm, and finally, the RANSAC algorithm is used for fine extraction of matching data. The whole algorithm process is named as the R-SIFT algorithm.) algorithms are used to extract and match the characteristics of the oil phase in oil-water two-phase flow to compare the advantages and disadvantages of three algorithms for oil phase velocity measurement. Analysis was carried out in this paper from three aspects: feature extraction, feature matching and processing, and oil phase average velocity.



a) velocity: 0.368 m/s, water cut: 90 %



b) velocity: 0.368 m/s, water cut: 80 %



c) velocity: 0.553 m/s, water cut: 90 %



d) velocity: 0.737 m/s, water cut: 90 %

Fig.10. PTV image of oil-water two-phase flow.

Table 2. Feature extraction and description.

Condition	Algorithm	Number of feature points		Computations for per feature point descriptor	Memory size of per descriptor	Number of matching point pairs	Time of description(ms)	
		1 st	2 nd				1 st	2 nd
a	R-SIFT	467	463	256rotation+ 256gradient+ 16mean	128 bytes	241	402.8	399.46
	R-ORB	678	692	512rotation	32 bytes	58	129.39	132.10
	P-OCRB	678	692	256rotation	32 bytes	378	64.69	66.03
b	R-SIFT	435	418	256rotation+ 256gradient+ 16mean	128 bytes	128	375.37	361.54
	R-ORB	701	678	512rotation	32 bytes	30	133.78	128.82
	P-OCRB	701	678	256rotation	32 bytes	306	66.89	64.38
c	R-SIFT	804	815	256rotation+ 256gradient+ 16mean	128 bytes	308	693.59	703.29
	R-ORB	1543	1565	512rotation	32 bytes	42	295.45	299.65
	P-OCRB	1543	1565	256rotation	32 bytes	805	147.24	149.35
d	R-SIFT	1098	1031	256rotation+ 256gradient+ 16mean	128 bytes	623	947.08	900.46
	R-ORB	2800	2664	512rotation	32 bytes	58	535.34	508.73
	P-OCRB	2800	2664	256rotation	32 bytes	1059	267.26	255.24

A. Feature detection and description processing

Under different conditions, two consecutive frames of oil-water two-phase flow images are randomly extracted and their feature points are extracted using the P-OCRB, the R-ORB, and the R-SIFT algorithms. By calculation, the feature points obtained by different algorithms for oil-water two-phase flow images under different conditions are shown in Table 2. Obviously, the number of feature points obtained by the R-SIFT algorithm is much smaller than that by the P-OCRB and the R-ORB algorithms. In addition, in the process of feature point detection in the R-SIFT algorithm, Gaussian blur is required first, and then 26-pixel points before and after the blur are compared to determine whether they are feature points. While the feature point detection in the P-OCRB and the R-ORB algorithms should be compared with 16-pixel points around them to determine whether they are feature points. It can be known that the R-SIFT algorithm has a much larger computational burden in detecting feature points than the P-OCRB and the R-ORB algorithms.

Then, the description calculation amount of each feature point for different algorithms in the description process is shown in Table 2. The feature point description process in the R-SIFT algorithm is much more complicated than that in the P-OCRB and the R-ORB algorithms. And the P-OCRB algorithm performed nearly half as much computations in the description process as the R-ORB algorithm. The R-SIFT algorithm descriptors are represented by 128-dimensional vectors, with each feature point descriptor occupying 128 bytes, while the P-OCRB and the R-ORB algorithm descriptors are represented by 256-bit binary code strings, with each feature point descriptor occupying 32 bytes.

Therefore, the order of ability used to detect a large number of features in the feature extraction process is as follows: P-OCRB = R-ORB > R-SIFT.

The order of complexity degree of each feature extraction process is as follows: R-SIFT > R-ORB > P-OCRB.

From the perspective of feature extraction, the P-OCRB algorithm has a comparative advantage, as it can not only extract a large number of feature points, but also improve the computational speed of feature description.

B. Feature matching and processing

After the feature extraction, feature matching is carried out, and then partial matching point pairs are extracted from all matching point pairs to improve the matching accuracy. The final matching results using the R-SIFT, the R-ORB, and the P-OCRB algorithms are shown in Fig.11. The red, green, and blue lines in the figure are the matching lines of the two frames of images. The left side of the line is the feature points in the first frame, and the right side of the line is the feature points in the corresponding matching second frame.

After analyzing and comparing three kinds of matching data, the comparison result is shown in Fig.12. The red and green lines in the figure are the matching data obtained by using the R-SIFT and the R-ORB algorithms, respectively.

The yellow line is the matching data extracted by the P-OCRB algorithm but not by the R-SIFT and the R-ORB algorithms. It can also be seen from Fig.11. that the number of matching point pairs using the P-OCRB algorithm is the largest, compared with the R-SIFT algorithm and the R-ORB algorithm. And there is no obvious error matching in the three figures. Therefore, the efficient order of feature matching results is P-OCRB>R-SIFT>R-ORB.

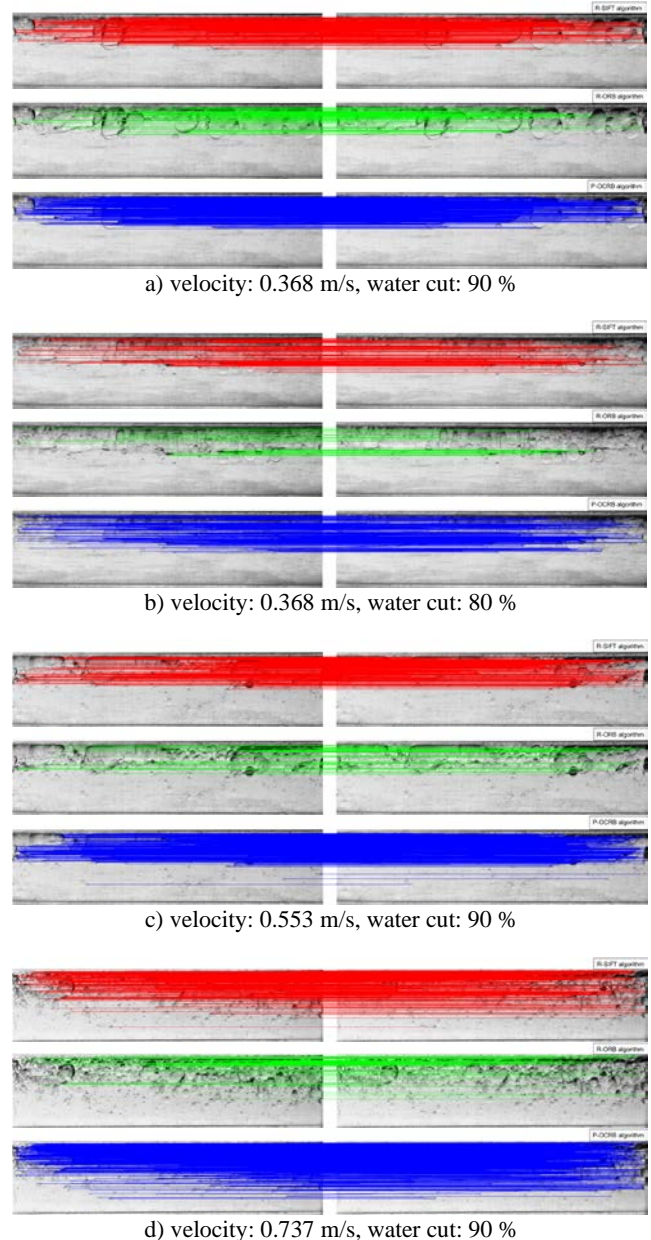


Fig.11. The matching results of using different algorithm.

Although the feature description of the SIFT algorithm is more accurate than that of the ORB algorithm, the accuracy of the two algorithms can be the same after using the RANSAC algorithm. The only drawback of the R-ORB algorithm is that it has fewer matching data. The P-OCRB algorithm not only makes up for the shortcomings of the R-

ORB algorithm, but also avoids the computational complexity of the R-SIFT algorithm. So, the P-OCRB algorithm is feasible in the velocity measurement of oil-water two-phase flow.

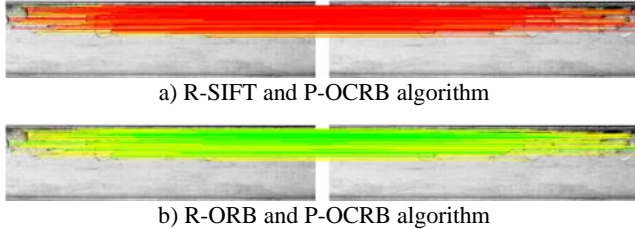


Fig.12. The Comparative analysis diagram.

C. Oil phase average velocity measurement

The average velocity of oil phase was measured according to three matching results. The average oil phase velocity and theory flow velocity calculated by the R-SIFT algorithm, the R-ORB algorithm, and the P-OCRB algorithm are shown in Fig.13. The R-SIFT algorithm is used for oil-water two-phase flow with flow velocity of 0.368 m/s, 0.553 m/s, 0.737 m/s, and 0.921 m/s to obtain the average error of oil phase flow velocity of 4.64 %, 4.25 %, 1.37 %, and 5.87 %, and the maximum error of 14.7 %, 9.68 %, 9.92 %, and 12.54 %, respectively. The R-ORB algorithm is used for oil-water two-phase flow with flow velocity of 0.368 m/s, 0.553 m/s, 0.737 m/s, and 0.921 m/s to obtain the average error of oil phase flow velocity of 11.12 %, 10.27 %, 12.28 %, and 10.36 %, and the maximum error of 22.7 %, 21.8 %, 20.2 %, and 24.9 %, respectively. The P-OCRB algorithm is used to obtain the average error of oil phase flow velocity of 4.12 %, 2.75 %, 2.51 %, and 2.36 %, and the maximum error of 13.7 %, 7.68 %, 8.29 %, and 5.39 %, respectively. And the measured data is stable around the actual data after

repeated experiments from two figures, and the variation coefficient of the experiment is 0.039. The smaller the variation coefficient, the higher the stability. Therefore, the stability of the P-OCRB algorithm is high.

A large number of experiments are carried out to observe the accuracy of the calculation results and the difference before and after algorithm improvement. The maximum errors of oil phase average velocity using the R-SIFT, the R-ORB, and the P-OCRB algorithms are calculated to be 9.42 %, 25.89 %, and 6.16 %, respectively. The average errors of the R-SIFT, the R-ORB, and the P-OCRB algorithms are 4.24 %, 13.34 %, and 1.2 %, respectively. Experimental data satisfies that the average oil phase velocity error calculated by the P-OCRB algorithm is generally lower than that calculated by the R-ORB and the R-SIFT algorithms.

The flow pattern of oil-water two-phase flow with high water cut and low velocity is in the state of oil-in-water in the upper layer and free water in the lower layer due to the influence of density. The oil phase is in an upward state and the average velocity of the oil phase is bound to be affected by the movement velocity of part of the oil phase. Therefore, the more characteristic matching data of oil phase, the more accurate matching results, and the smaller the average velocity error of oil phase. The P-OCRB algorithm not only improves the accuracy of the R-ORB algorithm in measuring the oil phase velocity, but also avoids the complexity and time consumption of the R-SIFT algorithm. And the relative errors obtained by the P-OCRB algorithm are all within the range of -6.5 %~6.5 %, which meets the allowable errors of instrument measurement. Therefore, the P-OCRB algorithm can be applied to the measurement of oil phase velocity in oil-water two-phase flow with low velocity and high water cut, and it can improve the calculation speed and accuracy of the oil phase velocity.

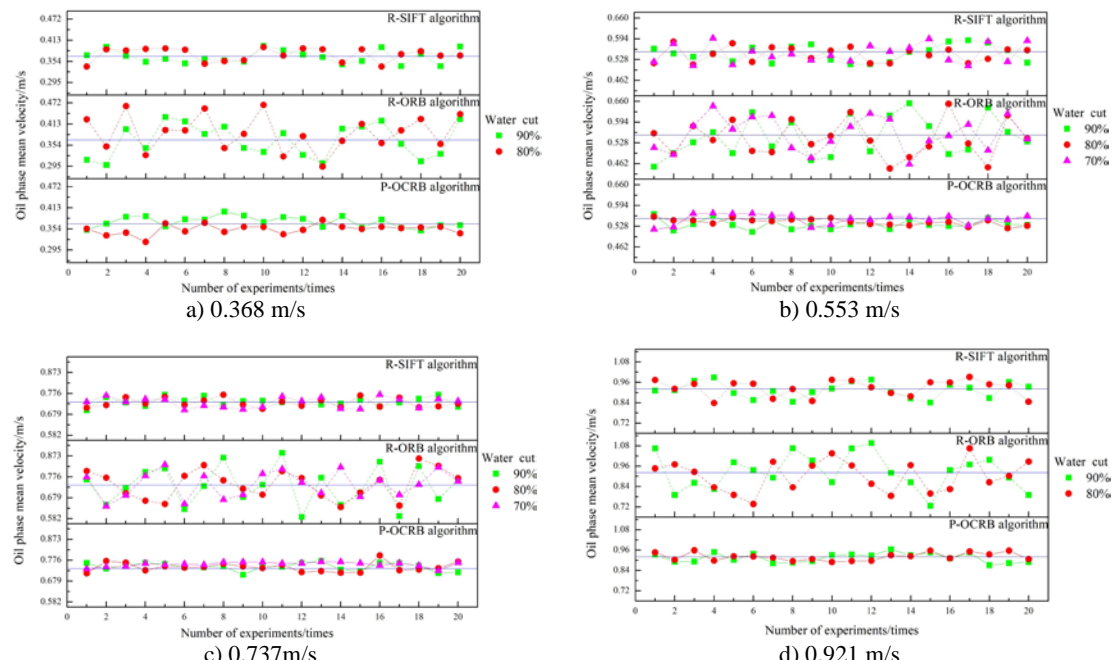


Fig.13. The Comparative analysis diagrams.

7. CONCLUSIONS

In this paper, the feature description of the ORB algorithm and the RANSAC algorithm is improved, and the improved algorithm is called the P-OCRB algorithm. The P-OCRB algorithm is applied to the measurement of oil phase velocity in oil-water two-phase flow with low velocity and high water cut. The following conclusions are obtained:

- 1) Compared with the R-SIFT and the R-ORB algorithms, the P-OCRB algorithm reduces the amount of computation, increases the number of matching points, and improves the accuracy of pixel matching.
- 2) The oil phase velocity measurement experiment of oil-water two-phase flow shows that the algorithm is stable and the velocity measurement errors are less than 6.16 %, far lower than those of the R-SIFT and the R-ORB algorithms.

ACKNOWLEDGMENT

This work was supported by the National Science Foundation of China (51774092), the China Postdoctoral Science Foundation (2016M601399) and Guiding Projects of Daqing (ZD-2019-05).

REFERENCES

- [1] Saoud, A., Mosorov, V., Grudzien, K. (2017). Measurement of velocity of gas/solid swirl flow using Electrical Capacitance Tomography and cross correlation technique. *Flow Measurement and Instrumentation*, 53, 133-140.
- [2] Dejam, M. (2019). Advection-diffusive-reactive solute transport due to non-Newtonian fluid flows in a fracture surrounded by a tight porous medium. *International Journal of Heat and Mass Transfer*, 128, 1307-1321.
- [3] Dejam, M., Hassanzadeh, H., Chen, Z. (2018). Semi-analytical solution for pressure transient analysis of a hydraulically fractured vertical well in a bounded dual-porosity reservoir. *Journal of Hydrology*, 565, 289-301.
- [4] Papi, A., Sharifi, A., Abdali, M.R. (2019). Simulation of the effect of rock type on recovery plan of a mature carbonate oilfield in the Middle East–Part 1: Waterflooding recovery plan. *Petroleum Science and Technology*, 37 (11), 1251-1259.
- [5] Gryzlov, A., Schiferli, W., Mudde, R.F. (2013). Soft-sensors: Model-based estimation of inflow in horizontal wells using the extended Kalman filter. *Flow Measurement and Instrumentation*, 34, 91-104.
- [6] Han, L., Hou, Y., Wang, Y., Liu, X., Han, J., Xie, R., Fu, C. (2019). Measurement of velocity of sand-containing Oil-Water two-phase flow with super high water holdup in horizontal small pipe based on thermal tracers. *Flow Measurement and Instrumentation*, 69, 101622.
- [7] Li, L., Kong, L., Xie, B., Fang, X., Kong, W., Liu, X., Zhao, F. (2019). The Influence on response of a combined capacitance sensor in horizontal oil–water two-phase flow. *Applied Sciences*, 9 (2), 346.
- [8] Wei, J.D., Jin, N.D., Lian, E.Y., Wang, D., Han, Y., Zhai, L. (2018). Measurement of water holdup in oil-in-water flows using three-channel conductance probe with center body. *IEEE Sensors Journal*, 18 (7), 2845-2852.
- [9] Xu, Z., Jiang, Y., Wang, B., Huang, Z., Ji, H., Li, H. (2017). Sensitivity distribution of CCERT sensor under different excitation patterns. *IEEE Access*, 5, 14830-14836.
- [10] Liu, C., Xu, L., Chen, J., Cao, Z., Lin, Y., Cai, W. (2015). Development of a fan-beam TDLAS-based tomographic sensor for rapid imaging of temperature and gas concentration. *Optics Express*, 23 (17), 22494-22511.
- [11] Aguirre-Pablo, A.A., Aljedaani, A.B., Xiong, J., Idoughi, R., Heidrich, W., Thoroddsen, S.T. (2019). Single-camera 3D PTV using particle intensities and structured light. *Experiments in Fluids*, 60 (2), 25.
- [12] Scharnowski, S., Bross, M., Kähler, C.J. (2019). Accurate turbulence level estimations using PIV/PTV. *Experiments in Fluids*, 60 (1).
- [13] Fu, S., Biwole, P.H., Mathis, C. (2016). Numerical and experimental comparison of 3D Particle Tracking Velocimetry (PTV) and Particle Image Velocimetry (PIV) accuracy for indoor airflow study. *Building and Environment*, 100, 40-49.
- [14] Rubbert, A., Schröder, W. (2020). Iterative particle matching for three-dimensional particle-tracking velocimetry. *Experiments in Fluids*, 61 (2), 58.
- [15] Gim, Y., Jang, D.K., Sohn, D.K., Kim, H., Ko, H.S. (2020). Three-dimensional particle tracking velocimetry using shallow neural network for real-time analysis. *Experiments in Fluids*, 61 (2), 1-8.
- [16] Qin, Y., Zou, J., Tang, B., Wang, Y., Chen, H. (2020). Transient feature extraction by the improved orthogonal matching pursuit and K-SVD algorithm with adaptive transient dictionary. *IEEE Transactions on Industrial Informatics*, 16 (1), 215-227.
- [17] Manickam, A., Devarasan, E., Manogaran, G., Priyan, M.K., Varatharajan, R., Hsu, C.H., Krishnamoorthi, R. (2019). Score level based latent fingerprint enhancement and matching using SIFT feature. *Multimedia Tools and Applications*, 78 (3), 3065-3085.
- [18] Ma, D., Lai, H.C. (2019). Remote sensing image matching based improved ORB in NSCT domain. *Journal of the Indian Society of Remote Sensing*, 47 (5), 801-807.
- [19] Kong, L.F., Kong, W.H., Li, Y.W., Zhang, C., Du, S.X. (2014). An improved particle image velocimetry algorithm for velocity measurement of oil-water two-phase flow. In *Applied Mechanics and Materials*. Trans Tech Publications Ltd., vol. 602, 1654-1659.

- [20] Yu, L., Yu, Z., Gong, Y. (2015). An improved ORB algorithm of extracting and matching. *International Journal of Signal Processing, Image Processing and Pattern Recognition*, 8 (5), 117-126.
- [21] Han, L., Wang, H., Liu, X., Xie, R., Mu, H., Fu, C. (2019). Particle image velocimetry of oil-water two-phase flow with high Water cut and low flow velocity in a Horizontal small-diameter pipe. *Sensors*, 19, 2702.
- [22] Pang, Y., Li, A. (2019). An improved ORB feature point image matching method based on PSO. In *Tenth International Conference on Graphics and Image Processing*. SPIE, vol. 11069.
- [23] Shu, C.W., Xiao, X.Z. (2018). Orb-oriented mismatching feature points elimination. In *2018 IEEE International Conference on Progress in Informatics and Computing*. IEEE, 246-249.
- [24] Rublee, E., Rabaud, V., Konolige, K., Bradski, G. (2011). ORB: An efficient alternative to SIFT or SURF. In *2011 International Conference on Computer Vision*. IEEE, 2564-2571.
- [25] Mohammad, S., Morris, T. (2017). Binary robust independent elementary feature features for texture segmentation. *Advanced Science Letters*, 23 (6), 5178-5182.
- [26] Wang, R., Xia, Y., Wang, G., Tian, J. (2015). License plate localization in complex scenes based on oriented FAST and rotated BRIEF feature. *Journal of Electronic Imaging*, 24 (5), 053011.
- [27] Bhat, A. (2017). Makeup invariant face recognition using features from accelerated segment test and eigen vectors. *International Journal of Image and Graphics*, 17 (1), 1750005.
- [28] Xu, J., Chang, H. W., Yang, S., Wang, M. (2012). Fast feature-based video stabilization without accumulative global motion estimation. *IEEE Transactions on Consumer Electronics*, 58 (3), 993-999.
- [29] Fotouhi, M., Hekmatian, H., Kashani-Nezhad, M.A., Kasaei, S. (2019). SC-RANSAC: Spatial consistency on RANSAC. *Multimedia Tools and Applications*, 78 (7), 9429-9461.
- [30] Fischler, M.A., Bolles, R.C. (1981). Random sample consensus: A paradigm for model fitting with applications to image analysis and automated cartography. *Communications of the ACM*, 24 (6), 381-395.
- [31] Mikolajczyk, K., Schmid, C. (2005). A performance evaluation of local descriptors. *IEEE Transactions on Pattern Analysis and Machine Intelligence*, 27 (10), 1615-1630.
- [32] Choi, S., Kim, T., Yu, W. (1997). Performance evaluation of RANSAC family. *Journal of Computer Vision*, 24 (3), 271-300.
- [33] Nistér, D. (2005). Preemptive RANSAC for live structure and motion estimation. *Machine Vision and Applications*, 16 (5), 321-329.

Received February 21, 2020

Accepted April 30, 2020